To Study the Structural, Optical and Magnetic Properties of Ni-Fe Doped ZnO Diluted Magnetic Semiconductors

Nakash Rizvi[1a], Abdul Rehman[2b], Muhammad Tahir Khan[1c]

[1]Department of Physics, Riphah International University, Islamabad, 44000, Pakistan

[2]Centre of Excellence in Solid State Physics, University of the Punjab Quaid-i-Azam Campus, Lahore, 54000, Punjab, Pakistan

Authors Email: [a]nakashrizvi@gmail.com, [b]abdulr71682@gmail.com, [c]mtahir.khan@riphah.edu.pk

Received: 21-12-2021, Received in Revised form: 13-03-2022
Accepted: 27-05-2022, Published: 30-06-2022

Abstract:

The nickel and iron co-doped with zinc oxide $Zn_{1-x-y}Fe_xNi_yO$ {(x=0, y=0), (x=0.05, y=0), (x=0, y=0.05), (x=0.03, y=0.02)} diluted magnetic semiconductor were successfully prepared by Sol-Gel technique. Pure and doped samples were characterized by X-ray diffraction, UV-visible spectroscopy, Vibrating Sample Magnetometer, and Fourier Transform Infrared Spectroscopy. The X-ray analysis of pure and doped ZnO confirmed the hexagonal wurtzite structure and no other phase like secondary and impurity. The UV-visible absorption spectra of Co-doped samples showed a blue shift in absorption edge as compared to un-doped or single-doped ZnO nanoparticles. The magnetic characterization confirms the room temperature ferromagnetism in all doped and co-doped ZnO nanoparticles. Magnetic saturation was improved in Fe-Ni Co-doped samples relative to pure or single doped with ZnO which reveals that the exchange interaction between Ni and Fe leads over the Ni-Ni and Fe-Fe ion interactions. The Fourier Transform Infrared Spectroscopy (FTIR) reveals the existence of chemical bonding and functional groups. It was confirmed that the occurrence of iron Fe and Ni modes is associated with the ZnO nanoparticles.

Keywords: Diluted Magnetic Semiconductors, Room Temperature Ferromagnetism, Ni, Fe co-doped ZnO, X-ray diffraction.

Introduction:

Diluted magnetic semiconductors (DMS) have attracted a lot of attracted in past years because it is a type of semiconductor in which magnetic ions are substituted against the host cations. It shows many applications in producing spintronic devices such as spin-valve transistors [1,2]. ZnO is a compound semiconductor in groups II-IV that has emerged as one of the most promising options for DMS materials [3]. Furthermore, ZnO has potential applications in optoelectronics due to its high exciton binding energy (60 meV) and wide bandgap (3.37 eV) properties have potential uses in optoelectronics. In recent years, scientists have been studying the effects of doping transition metals including Co, Mn, Fe, and Ni into ZnO nanoparticles [4]. Many theories have suggested and confirmed that doping these transition elements into ZnO nanoparticles causes significant changes in luminous and magnetic characteristics. These transition metals have been doped on ZnO lattice to change the different magnetic and optical properties, which might be used in spintronic devices, such as quantum computers, gas sensors, and spin field-effect transistors. To achieve these goals, it is critical to develop ZnO-based ferromagnetic materials with well-understood physical and structural characteristics. The ferromagnetism strongly depends on environmental conditions and the synthesis method used for the preparation of samples which is confirmed by the experiments [5]. In recent, many reported on ZnO with single transition metal-doped prepared by different methods such as Mn–Co codoped [6], Fe-Ni codoped [7], Fe–Co codoped [8], Co–Cu codoped, and Cr–Fe codoped [9]. In recent, there are many other reported, magnesium doped with nano ferrites [10], calcium chromium magnesium nano ferrites [11], Ce-doped Co-Mg-Cd spinel nano-ferrites [12]. Many processes have been discovered to synthesize the nanostructure, they are co-precipitation [13], sol-gel [14], solvothermal [15,16,17,18], sonochemical [19-20], and polymeric citrate precursor [21].

In this work, the sol-gel method was chosen for synthesis because it has high purity and good uniformity. It is energy-saving because of the low annealing temperature. It can easily use for the preparation of composite, coating, and fiber materials. The effect of doping materials Ni and Fe with the ZnO nanoparticles on the structural, optical, magnetic, and chemical bonding properties were examined by using X-ray diffraction (XRD), UV-Vis spectroscopy, vibrating sample magnetometer (VSM), Fourier Transform Infrared Spectroscopy (FTIR) respectively.

The experimental result showed that the co-doping of Ni and Fe with ZnO nanoparticles has increased the properties of ferromagnetic material. It was also observed that the change in lattice constant in structure studies and optical properties.

Experimental Procedure:

All the materials were purified and analytical reagent grade which is used in this work. To synthesize the pure ZnO nanoparticles, zinc acetate ($Zn(CH_3COO)_2{\cdot}2H_2O$) was added in De-ionized water and stirred for 1 h. In this solution, citric acid ($C_6H_8O_7$) and Ethylene glycol ($C_2H_6O_2$) was added in a solution for making the reaction fast. An aqueous solution of ammonia (NH_3) was added dropwise to the solution to maintain the pH ~11, and the color change into greenish-yellow from reddish-orange. To make the gel form, the solution was stirred at room temperature and dried at 120℃ for 3 hours, the color changed into blackish-brown, grind it to make the fine powder. To remove the unwanted chemicals, and make the oxide of the fine powder, annealing it into the furnace at 650 ℃ for 2 hours. To synthesize the doped $Zn_{1-x-y}Fe_xNi_yO$ {(x=0.05, y=0), (x=0, y=0.05), (x=0.03, y=0.02)} nanoparticles, the same steps have been repeated except adding nickel acetate ($C_4H_6NiO_4.4H_2O$) and iron nitrate ($FeNO_3$) according to the calculated stoichiometric ratio as shown in figure 1.

Figure 1: Synthesis process of iron-nickel co-doped with zinc oxide nanoparticle by sol-gel method

https://doi.org/10.24949/njes.v15i1.678

Results and Discussion:

X-ray diffraction Analysis:

The pattern of $Zn_{1-x-y}Fe_xNi_yO$ {(x=0, y=0), (x=0.05, y=0), (x=0, y=0.05), (x=0.03, y=0.02)} are shown in figure 2(a), and (b). XRD diffraction peaks having different diffractions labeled as (100), (002), (101), (102), (110), (103), (200), (112), (201), and (202) shows the planes in one phase with the structure of hexagonal wurtzite. The diffraction peaks of the XRD graphs are matched with the standard spectrum (JCPDS card number 01-079-2205). There are no secondary phases and no traces of impurity in the detection limit of XRD. The result shows that Ni and Fe ions are well incorporated within the lattice of the host material. The product formed clearly shows that there is a pure phase and has no characteristics peaks are found from the other impurities. The narrow width and strong intensity of XRD results exhibit a good crystalline structure. We calculate the average size of grain can be calculated from the full-width half-maximum of major diffraction peak (101), we calculate it by using the Scherer formula.

$$D = \frac{K\lambda}{B\cos\theta} \quad (1)$$

Where 'D' shows the size of grain (hkl) shows an index of crystals and 'K' is Scherer's shape-related constant, 'λ' is the wavelength of X-ray, 'B' is the FWHM (Full width at half maximum) and 'θ' is the angle of diffraction of the peak. Results are displayed in table 1: the average crystalline size of co-doped ZnO nanoparticles is 38.86 nm which is smaller than the pure ZnO nanoparticles 44.53 nm. For co-doped Ni and Fe with ZnO the peaks shift toward lower angles as compared with the pure ZnO and also the peak intensity decreases in the Fe and Ni-doped concentration. This shifting and decrease in peaks show that Ni and Fe are well incorporated with the pure ZnO as shown in figure 2(a) the peaks shift to a lower angle because according to equation $\lambda = 2d_{hkl}\sin\theta$ when d changes its lattice parameter changes and that's why the peak shifts in doped material as shown in figure 2(b). The peaks can also be affected by the orientation of the sample and the temperature provided to it. By using Bragg's formula.

$$\lambda = 2d_{hkl}\sin\theta \quad (2)$$

We can find wavelength 'λ'. Where d_{hkl} represents crystalline plane distance with indices (hkl) and 'θ' represents the angle of diffraction of peak (101). The results show that the value of crystalline distance d of doped ZnO is almost constant. The lattice constant can be determined by using the relation.

$$a = d_{hkl}\sqrt{\frac{4}{3}(h^2 + hk + l^2) + \left(\frac{a}{c}\right)^2 l^2} \quad (3)$$

Where 'a' and 'c' are lattice constants and 'd_{hkl}' is a distance of crystalline plane with indices (hkl). The values of these parameters are displayed in table 1 [22].

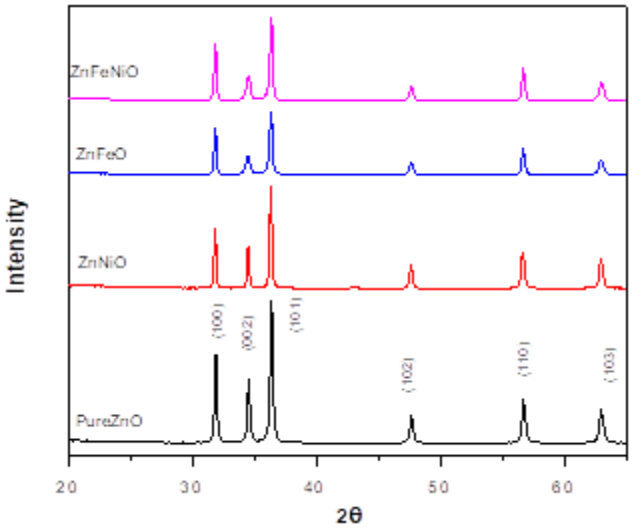

Figure 2 (a): XRD Pattern of Pure ZnO, ZnNiO, ZnFeO, and ZnNiFeO Nanoparticles

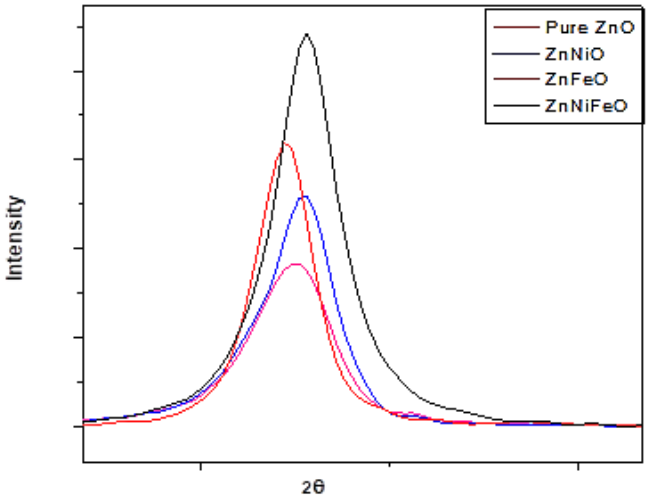

Figure 2 (b): XRD Pattern Shift of Pure ZnO, ZnNiO, ZnFeO, and ZnNiFeO Nanoparticles

Table 1: Calculations of XRD Data.

Sample	2θ	d	a(Å)	D(nm)
Pure ZnO	31.8	0.281064	0.1405319	45.872782
	34.44	0.260099	0.5201973	43.757151
	36.28	0.247318	0.2473181	43.981715
ZnNiO	31.74	0.281581	0.1407906	51.599191
	34.43	0.260245	0.5204904	51.958835
	36.22	0.247714	0.2477141	49.147611
ZnFeO	31.76	0.281408	0.1407042	45.868224
	34.40	0.260392	0.5207839	24.449895
	36.26	0.247449	0.2474499	34.816868
ZnNiFeO	31.76	0.281408	0.1407043	51.601752
	34.46	0.259952	0.5199045	25.194888
	36.28	0.247318	0.2473180	39.792981

Ultraviolet-Visible Spectroscopy:

The Ultraviolent absorption spectroscopy was used for analyzing the optical properties of the sample being synthesized

$Zn_{1-x-y}Fe_xNi_yO$ {(x=0, y=0), (x=0.05, y=0), (x=0, y=0.05), (x=0.03, y=0.02)}. The absorption effects of different peaks are shown in figure 3 (a) and calculations of the absorbance data are shown in table 2. By increasing the concentrations of Ni and Fe doping with pure ZnO, then the absorption edge of the doped samples occurs blue-shift. This is due to the Ni^{2+} and Fe^{2+} ions replacing the position of Zn^{2+} in the ZnO lattice. The position of Zn^{+2} is replaced by Ni^{+2} and Fe^{+2}. The tauc gap rule is used for studying the optical properties of amorphous solid materials. The Tauc graph shows the absorption of light energy (hv) and this energy bandgap is measured by using equation

$$(\alpha hv)^2 = A(hv - E_g) \quad (4)$$

In which 'hv' shows the energy of photons, 'v' shows the frequency of photons and 'E_g' is the energy of bandgap.

$$A = \frac{4\pi k}{\lambda} \quad (5)$$

It shows the absorption coefficient. 'λ' and 'k' are wavelength and absorbency and 'h' is Planck's constant. For direct transition, we chose the square of 'αhv'. It gives us the best-fitting linear curve for the region of the band edge. The relation between hv and $(\alpha hv)^2$ is shown in figure 3(b). We can find the E_g values by extrapolating the linear region near onset in the plot of hv verses $(\alpha hv)^2$. The values of bandgap E_g are 2.8721 eV, 2.4784 eV, 2.7159 eV and 2.4159 eV for ZnO pure, $Zn_{0.95}Fe_{0.05}O$ $Zn_{0.95}Ni_{0.05}O$ and $Zn_{0.95}Fe_{0.03}Ni_{0.02}O$ respectively. By comparing the bandgap of doped ZnO of Fe and Ni with the pure ZnO it probably is seen that doped ZnO is lowering gradually. The optical (UV) bandgap gradually decreases in the transition metal because of the sp-d exchange of spin interaction between localized d-subshell electrons and band electrons of transition metal ions that are substituting cation. Thus the Ni and Fe samples are entered into the ZnO lattice site, the p-d and s-d interactions exchange between localized d electrons and ZnO band electrons of Ni and Fe give rise to the change in the structure of the energy band respectively, it leads to the reduction in the bandgap as shown in figure 3 (b) and calculations of the bandgap data shown in table 2 [23].

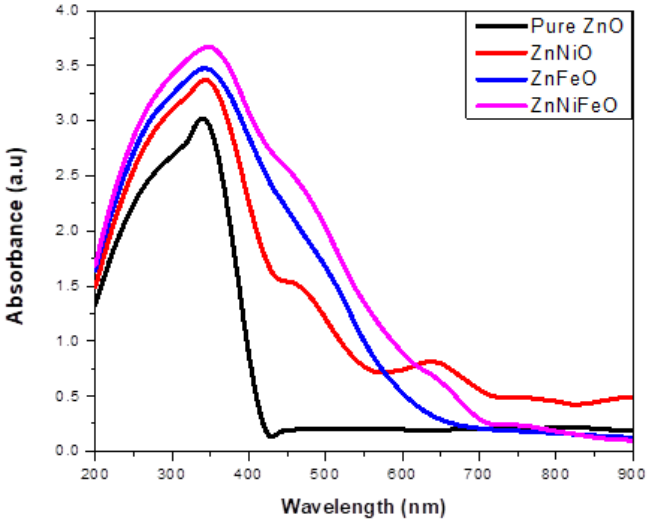

Figure 3 (a): Absorbance of ZnO, ZnNiO, ZnFeO, and ZnNiFeO Nanoparticles

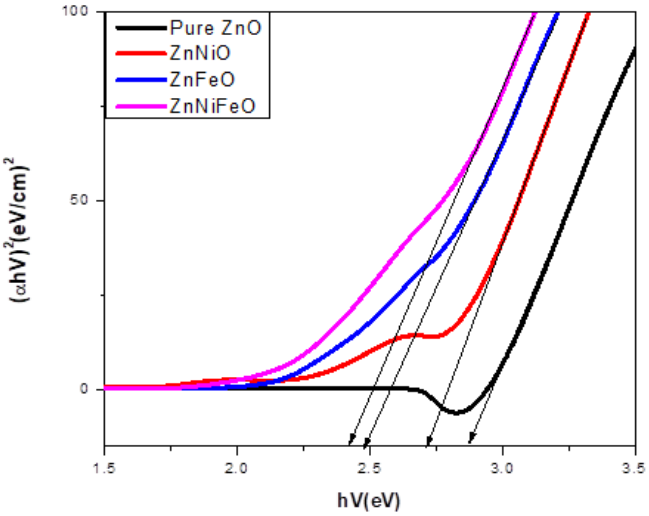

Figure 3 (b): Band Gap of ZnO, ZnNiO, ZnFeO, and ZnNiFeO Nanoparticles

Table 2: Calculation of Absorbance, and Band Gap of UV data

Sample	Absorbance (a.u)	Wavelength (nm)	Band Gap (E_g)
ZnO pure	3.023	338.990	2.8721 eV
ZnFeO	3.480	341.178	2.4784 eV
ZnNiO	3.374	341.178	2.7159 eV
ZnFeNiO	3.663	345.553	2.4159 eV

Vibrating Sample Magnetometer (VSM):

The room temp ferromagnetism RTFM of the $Zn_{1-x-y}Fe_xNi_yO$ {(x=0, y=0), (x=0.05, y=0), (x=0, y=0.05), (x=0.03, y=0.02)} pure and doped samples was prepared. Therefore the achieved ferromagnetic behavior is an extrinsic characteristic of $Zn_{0.95}Fe_{0.05-x}Ni_xO$ nanoparticles. Figure 4 exhibits magnetic Hysteresis loops of doped and pure samples that are evaluated at room temperature. It is clearly shown from the loops that nanoparticles of pure ZnO possess feeble paramagnetic behavior at room temperature. On the other hand, all doped and co-doped samples show ferromagnetism. The saturated values of magnetization are 0.015208 emu/g, 0.018999 emu/g, 0.017069 emu/g, and 0.012606 emu/g respectively for pure ZnO, $Zn_{0.95}Ni_{0.05}O$, $Zn_{0.95}Fe_{0.05}O$, and $Zn_{0.95}Fe_{0.03}Ni_{0.02}O$ and Coercivity are 204.1917 Oe, 223.5210 Oe, 83.43977 Oe, and 83.41429 Oe respectively. Both the coercivity and saturation magnetization of the Co-doped sample is small as compared to un-doped individual doped samples as shown in figure 4 and the calculation of the hysteresis curve is shown in table 3.

It is perceptible from results of UV and XRD that iron Fe and nickel Ni are well merged into ZnO nanoparticles lattice, the basis of magnetism in the results is because of substitution among local spin polarize electrons and conduction electrons.

Local spin effects due to the delocalized and localized electrons. P-d coupling is a reaction that occurs where two fragments are fused with the assistance of a metal substance. This type is discussed in the category of organometallic compounds. In this type, the bonding is between organic and metallic compounds. It might be able to spin polarization of conduction electrons. As a result, later a consecutively long-range exchange interaction, nearly all Ni^{2+}, and Fe^{2+} ions reveal a similar spin direction, leading towards the ferromagnetic material [24, 25, 26].

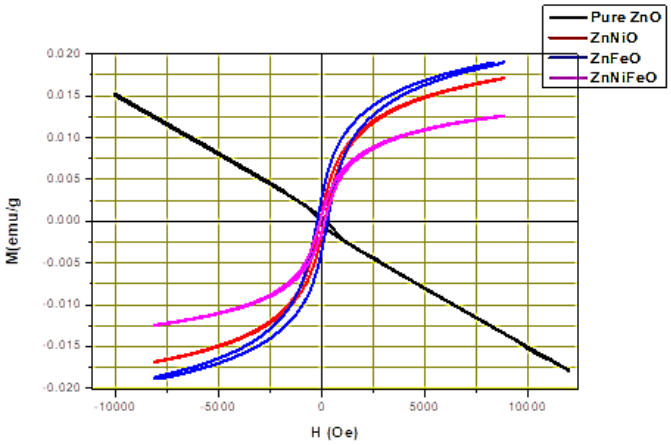

Figure 4: Comparison of VSM Graph of $Zn_{1-x-y}Fe_xNi_yO$

Table 3: Calculation of VSM Data

Sample	Magnetic Saturation Value (Ms)	Coercivity (Hc)
Pure ZnO	0.015208 emu/g	204.1917 Oe
ZnFeO	0.018999 emu/g	223.5210 Oe
ZnNiO	0.017069 emu/g	83.43977 Oe
ZnFeNiO	0.012606 emu/g	83.41429 Oe

Fourier Transform Infrared Spectroscopy (FTIR):

FTIR spectrum of $Zn_{1-x-y}Fe_xNi_yO$ {(x=0, y=0), (x=0.05, y=0), (x=0, y=0.05), (x=0.03, y=0.02)} nanoparticles prepared by sol-gel method. The range of the sample is measured from 3000 to 1000 cm^{-1} at room temperature. The band position and intensity of peak are relays on chemical composition, crystal structure, and sample morphology. The infrared absorption peak is found from FTIR spectra, near 1506 cm^{-1}, which shows that the peaks are metal oxide fingerprint range. Sharp peaks detected at 2340 cm^{-1}, which shows that strong stretching of O=C=O bond, and C-H bending shows a week in nature at 1982 cm^{-1}. In addition, the wurtzite structure can be identified by the peak at 399-416 cm^{-1}, assigned to a Zn−O bond. The FT-IR spectra of all the samples were not changed with the addition of Ni^{2+} and Fe^{+2} doping concentrations. The doping ions were successfully substituted for the lattice site of Zn^{2+} and into the ZnO host lattice without changing the crystal structure. This result is on a good promise with the result of XRD as shown in figure 5 [27,28].

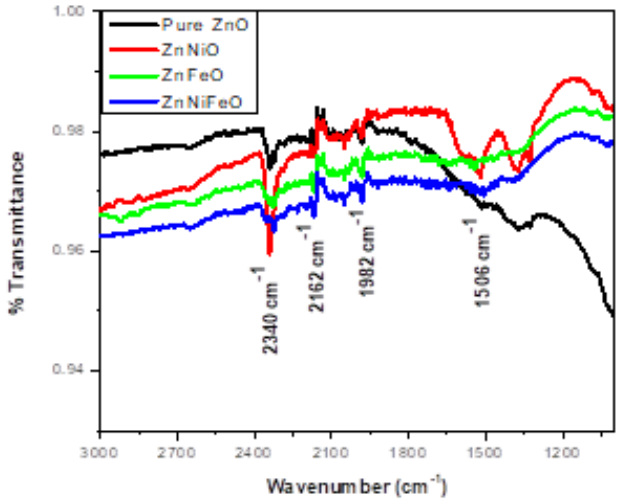

Figure 5: FTIR Graph of Sample ZnO, ZnNiO, ZnFeO, and ZnNFO

Table 4: FTIR Peaks and their assignments for the Zn1-x-yFexNiyO

Assignments	ZnO	ZnNiO	ZnFeO	ZnFeNiO
Stretching Zn-O	416.57 cm^{-1}	407.24 cm^{-1}	397.9 cm^{-1}	399.18 cm^{-1}

Conclusion:

$Zn_{1-x-y}Fe_xNi_yO$ {(x=0, y=0), (x=0.05, y=0), (x=0, y=0.05), (x=0.03, y=0.02)} diluted magnetic semiconductor nanoparticles were prepared by sol-gel method. For the analysis of structural, optical, magnetic, and chemical properties by using X-ray diffraction, Ultraviolet-Visible Spectroscopy, Vibrating Sample Magnetometer, and Fourier Transform Infrared Spectroscopy, respectively. The XRD shows a hexagonal wurtzite structure with no impurity phases for all samples. The Ni, Fe, and Ni-Fe doped samples are shows the blue shift in wavelength, due to the Ni^{2+} and Fe^{2+} ions replace in Zn^{+2} which is analyzed by using UV absorption spectrum. It was confirmed that the bandgap and optical absorption of ZnO nanoparticles can be controlled by doped and co-doped. The decrease in band gap due to p-d and s-d interactions exchange between localized d electrons and ZnO band electrons of Ni and Fe. The co-doped of Ni-Fe shows the increase in room temperature ferromagnetism RTFM as compared to single doped samples with ZnO nanoparticles which are observed in M-H measurement. It was observed that the ferromagnetic behavior shows in co-doped due to oxygen intermediated exchange interaction. Such as Ni-O-Fe, and Ni-O-Ni exchange interaction controls the Ni-O-Ni and Fe-O-Fe which effects on increasing the saturation magnetization at room temperature. The vibrational modes of ZnO with the chemical bonding without any modes related to doping samples are revealed by FTIR. The co-doped sample shows higher optical transmittance and the spectra of all the samples were not changed with the addition of doping because doping ions were successfully substituted for the lattice site of Zn^{2+}.

References:

1. Sharma, P. (2005). How to create a spin current. Science, 307(5709), 531-533.
2. Sharifi, A., Motlagh, S. Y., & Badfar, H. (2019). Ferro hydro dynamic analysis of heat transfer and biomagnetic fluid flow in channel under the effect of two inclined permanent magnets. Journal of Magnetism and Magnetic Materials, 472, 115-122.
3. Dietl, T., Ohno, O. H., Matsukura, A. F., Cibert, J., & Ferrand, E. D. (2000). Zener model description of ferromagnetism in zinc-blende magnetic semiconductors. science, 287(5455), 1019-1022.
4. Wesselinowa, J. M., & Apostolov, A. T. (2010). A possibility to obtain room temperature ferromagnetism by transition metal doping of ZnO nanoparticles. Journal of Applied Physics, 107(5), 053917.
5. Mandal, S. K., Das, A. K., Nath, T. K., Karmakar, D., & Satpati, B. (2006). Microstructural and magnetic properties of ZnO: TM (TM= Co, Mn) diluted magnetic semiconducting nanoparticles. Journal of applied physics, 100(10), 104315.
6. Sharma, V. K., Najim, M., Srivastava, A. K., & Varma, G. D. (2012). Structural and magnetic studies on transition metal (Mn, Co) doped ZnO nanoparticles. Journal of magnetism and magnetic materials, 324(5), 683-689.
7. Wu, X., Wei, Z., Zhang, L., Zhang, C., Yang, H., & Jiang, J. (2014). Synthesis and characterization of Fe and Ni co-doped ZnO nanorods synthesized by a hydrothermal method. Ceramics International, 40(9), 14635-14640.
8. Yu, X., Meng, D., Liu, C., He, X., Wang, Y., & Xie, J. (2012). Structure and ferromagnetism of Fe-doped and Fe-and Co-codoped ZnO nanoparticles synthesized by homogeneous precipitation method. Materials Letters, 86, 112-114.
9. Chand, P., Gaur, A., & Kumar, A. (2014). Effect of Cr and Fe doping on the structural and optical properties of ZnO nanostructures. Int. J. Chem. Nucl. Mater. Metall. Eng., 8, 1238-1241.
10. Nosheen, Sumaira, Sadia Sagar Iqbal, Muhammad Irfan, Aneela Sabir, Rafiullah Khan, and Tasawar Shahzad. "Impact of Mg Ion Doping on the Structural, Morphological, Thermal, Electrical and Dielectric Properties of Bismuth Cobalt Nanoferrites." Arabian Journal for Science and Engineering (2021): 1-6.
11. Nosheen, S., Iqbal, S. S., Bahadar, A., Hossain, N., & Shahzad, T. (2021). Fabrication & characterization of novel conductive nanomaterial, $Ca_xCr_{0.5-x}Mg_{0.5}Fe_2O_4$. Korean Journal of Chemical Engineering, 38(12), 2536-2540.
12. Zakir, R., Iqbal, S. S., Rehman, A. U., Nosheen, S., Ahmad, T. S., Ehsan, N., & Inam, F. (2021). Spectral, electrical, and dielectric characterization of Ce-doped Co-Mg-Cd spinel nano-ferrites synthesized by the sol-gel auto combustion method. Ceramics International, 47(20), 28575-28583.
13. V. A. L. Roy, A. B. Djurisic, H. Liu, X. X. Zhang, Y. H. Leung, M. H. Xie, J. Gao, H. F. Lui, C. Surya, Magnetic properties of Mn doped ZnO tetrapod structures, Appl. Phys. Lett.84 (2004) 756-758.
14. D. P. Joseph, G. S. Kumar, C. Venkateswaran, Structural, magnetic and optical studies of $Zn_{0.95}Mn_{0.05}O$ DMS, Mater. Lett. 59 (2005) 2720-2724.
15. Y. M. Kim, M. Yoon, I. W. Park, Y. J. Park, J. H. Lyou, Synthesis and magnetic properties of $Zn_{1-x}Mn_xO$ films prepared by the sol-gel method, Solid State Commun. 129 (2004) 175-178.
16. I. A. Wani, S. Khatoon, A. Ganguly, J. Ahmed, A. K. Ganguli, T. Ahmad, Silver nanoparticles: Large scale solvothermal synthesis and optical properties, Mater. Res. Bull. 45 (2010) 1033-1038.
17. T. Ahmad, S. Khatoon, K. Coolahan, Optical, magnetic and structural characterization of Zn1-xCoxO nanoparticles synthesized by solvothermal method, Bull. Mater. Sci. Accepted,Ms. No. BOMS-D-12-00330R1 (2013).
18. S. Khatoon, T. Ahmad, Synthesis, Optical and Magnetic properties of Ni-doped ZnO nanoparticles, J. Mat. Sci. Eng. B 2(6) (2012) 325-333.
19. S. Khatoon, K. Coolahan, S. E. Lofland, T. Ahmad, Optical and magnetic properties of solid solutions of $In_{2-x}Mn_xO_3$ (0.05, 0.10 and 0.15) nanoparticles, J. Alloy. Compd. 545 (2012) 162-167.
20. I. A. Wani, A. Ganguly, J. Ahmed, T. Ahmad, Silver nanoparticles: Ultrasonic wave assisted synthesis, optical characterization and surface area studies, Mater. Lett. 65 (2011) 520-522.
21. I. A. Wani, T. Ahmad, Size and shape dependant antifungal activity of gold nanoparticles: A case study of Candida, Colloid. Surface. B 101 (2013) 162–170.
22. K Sharma, V., & Varma, G. D. (2012). Fe clusters as origin of ferromagnetism in hydrogenated $Zn_{1-x}Fe_xO$ (x= 0.02 & 0.05) samples. Advanced Materials Letters, 3(2), 126-129.

23. Ciciliati, M. A., Silva, M. F., Fernandes, D. M., de Melo, M. A., Hechenleitner, A. A. W., & Pineda, E. A. (2015). Fe-doped ZnO nanoparticles: synthesis by a modified sol–gel method and characterization. Materials Letters, 159, 84-86.
24. Bates, R. (2012). Organic synthesis using transition metals. John Wiley & Sons.
25. Snieckus, V. (2016). New Trends in Cross-Coupling: Theory and Applications. Johnson Matthey's international journal of research exploring science and technology in industrial applications, 99.
26. Lipshultz, J. M., Li, G., & Radosevich, A. T. (2021). Main Group Redox Catalysis of Organopnictogens: Vertical Periodic Trends and Emerging Opportunities in Group 15. Journal of the American Chemical Society, 143(4), 1699-1721.
27. Irshad, K., Khan, M. T., & Murtaza, A. (2018). Synthesis and characterization of transition-metals-doped ZnO nanoparticles by sol-gel auto-combustion method. Physica B: Condensed Matter, 543, 1-6.
28. Wu, M., Wei, Z., Zhao, W., Wang, X., & Jiang, J. (2017). Optical and magnetic properties of Ni doped ZnS diluted magnetic semiconductors synthesized by hydrothermal method. Journal of Nanomaterials, 2017.